Enhanced Ca^{2+} signaling, mild primary aldosteronism, and hypertension in a familial hyperaldosteronism mouse model (*Cacna1h$^{M1560V/+}$*)

Eric Seidel[a,b,c,d] ![ORCID], Julia Schewe[a,b,c,d] ![ORCID], Junhui Zhang[e] ![ORCID], Hoang An Dinh[a,b,c] ![ORCID], Sofia K. Forslund[b,f,g,h] ![ORCID], Lajos Markó[b,f,g] ![ORCID], Nicole Hellmig[a,b,c], Jörg Peters[i], Dominik N. Muller[b,f,g], Richard P. Lifton[e,j,1], Timothy Nottoli[k] ![ORCID], Gabriel Stölting[a,b,c] ![ORCID], and Ute I. Scholl[a,b,c,d,1] ![ORCID]

aDepartment of Nephrology, Charité–Universitätsmedizin Berlin, 10115 Berlin, Germany; bBerlin Institute of Health at Charité–Universitätsmedizin Berlin, 10117 Berlin, Germany; cCenter for Regenerative Therapies, Berlin Institute of Health at Charité–Universitätsmedizin Berlin, 13353 Berlin, Germany; dDepartment of Nephrology, School of Medicine, Heinrich-Heine Universität Düsseldorf, 40225 Düsseldorf, Germany; eDepartment of Genetics, Yale University School of Medicine, New Haven, CT 06519; fMax Delbrück Center for Molecular Medicine, Helmholtz Association of German Research Centers, 13125 Berlin, Germany; gExperimental and Clinical Research Center, Max Delbrück Center for Molecular Medicine, Charité-Universitätsmedizin Berlin, 13125 Berlin, Germany; hDZHK (German Centre for Cardiovascular Research), Partner Site Berlin, 13019 Berlin, Germany; iDepartment of Physiology, Universitätsmedizin Greifswald, 17475 Greifswald, Germany; jLaboratory of Human Genetics and Genomics, The Rockefeller University, New York, NY 10065; and kSection of Comparative Medicine, Yale Genome Editing Center, Yale University School of Medicine, New Haven, CT 06519

Gain-of-function mutations in the *CACNA1H* gene (encoding the T-type calcium channel Ca$_V$3.2) cause autosomal-dominant familial hyperaldosteronism type IV (FH-IV) and early-onset hypertension in humans. We used CRISPR/Cas9 to generate *Cacna1h$^{M1560V/+}$* knockin mice as a model of the most common FH-IV mutation, along with corresponding knockout mice (*Cacna1h$^{-/-}$*). Adrenal morphology of both *Cacna1h$^{M1560V/+}$* and *Cacna1h$^{-/-}$* mice was normal. *Cacna1h$^{M1560V/+}$* mice had elevated aldosterone:renin ratios (a screening parameter for primary aldosteronism). Their adrenal *Cyp11b2* (aldosterone synthase) expression was increased and remained elevated on a high-salt diet (relative autonomy, characteristic of primary aldosteronism), but plasma aldosterone was only elevated in male animals. The systolic blood pressure of *Cacna1h$^{M1560V/+}$* mice was 8 mmHg higher than in wild-type littermates and remained elevated on a high-salt diet. *Cacna1h$^{-/-}$* mice had elevated renal *Ren1* (renin-1) expression but normal adrenal *Cyp11b2* levels, suggesting that in the absence of Ca$_V$3.2, stimulation of the renin-angiotensin system activates alternative calcium entry pathways to maintain normal aldosterone production. On a cellular level, *Cacna1h$^{M1560V/+}$* adrenal slices showed increased baseline and peak intracellular calcium concentrations in the zona glomerulosa compared to controls, but the frequency of calcium spikes did not rise. We conclude that FH-IV, on a molecular level, is caused by elevated intracellular Ca^{2+} concentrations as a signal for aldosterone production in adrenal glomerulosa cells. We demonstrate that a germline *Cacna1h* gain-of-function mutation is sufficient to cause mild primary aldosteronism, whereas loss of Ca$_V$3.2 channel function can be compensated for in a chronic setting.

Ca$_V$3.2 | calcium imaging | adrenal gland

As a key regulator of blood pressure and electrolyte homeostasis, the mineralocorticoid hormone aldosterone is synthesized from its precursor cholesterol in the zona glomerulosa of the adrenal cortex. Cortisol and aldosterone differ by modification at C-17 in cortisol and C-18 in aldosterone. C-18 modification is catalyzed by aldosterone synthase (encoded by the *CYP11B2* gene in humans). Altered *CYP11B2* expression governs chronic changes in aldosterone production (1). The two main physiological stimuli of aldosterone production are volume depletion and elevated blood potassium (hyperkalemia). Volume depletion activates the renin-angiotensin system (RAS), leading to production of the peptide hormone angiotensin II (Ang II). Ang II binds to its selective G protein-coupled receptor in the zona glomerulosa, triggering calcium release from intracellular stores, depolarizing cells by inhibition of potassium channels, and activating voltage-gated calcium influx from the extracellular space. Hyperkalemia directly depolarizes glomerulosa cells, similarly promoting calcium entry. The resulting elevated intracellular calcium levels are the key signal for aldosterone production (1, 2). In response to aldosterone, the kidney increases NaCl reabsorption and potassium secretion, restoring balance.

When increased production of aldosterone is at least partially uncoupled from its main physiological stimuli, primary aldosteronism ensues. This disorder is present in about 6% of hypertensives in a primary care setting and is thus considered the most prevalent

Significance

Primary aldosteronism (increased production of the adrenal steroid hormone aldosterone) is the most common cause of secondary hypertension. We here generated a mouse model of familial hyperaldosteronism type IV with a heterozygous gain-of-function mutation in a calcium channel gene (*Cacna1h$^{M1560V/+}$*). *Cacna1h$^{M1560V/+}$* mice have about twofold elevated aldosterone:renin ratios (a screening parameter for primary aldosteronism) and elevated blood pressure, with an overall mild phenotype. Elevated adrenal aldosterone synthase expression in *Cacna1h$^{M1560V/+}$* mice is associated with increased intracellular calcium concentrations in glomerulosa cells. This model allows for the ex vivo analysis of calcium signaling in aldosterone-producing glomerulosa cells of the adrenal gland. *Cacna1h$^{-/-}$* mice have normal aldosterone synthase expression, with implications for the evaluation of CACNA1H as a therapeutic target.

cause of secondary hypertension (3). Its diagnosis is based on an elevated aldosterone:renin ratio (ARR) and a positive confirmatory test, such as the failure to suppress aldosterone levels upon administration of NaCl ("saline suppression test") (4). About one-third of patients with primary aldosteronism have a benign tumor of the adrenal gland (aldosterone-producing adenoma, APA), and the majority of the remainder have bilateral adrenal hyperplasia (4). On a molecular level, about 90% of APAs are explained by heterozygous or hemizygous somatic mutations in one of seven genes (5–7). Mutations in L-type (CACNA1D) (8, 9) and T-type (CACNA1H) (10) calcium channel genes directly cause increased calcium influx (8, 11). Mutations in other ion channels [KCNJ5 (12), CLCN2 (13)] and ion pump genes (ATP1A1, ATP2B3) (14) depolarize the cell membrane and indirectly increase voltage-gated calcium influx. CTNNB1 (15) mutations prevent differentiation of glomerulosa cells into fasciculata cells, leading to increased glomerulosa cell mass (16).

In addition, recent studies suggest that somatic mutations in APA genes, in particular CACNA1D and ATP1A1, can cause so-called aldosterone-producing cell clusters, small nodules that protrude into the zona fasciculata and occur in healthy subjects (17) and, more prominently, in subjects with bilateral adrenal hyperplasia (18, 19). Heterozygous mutations in APA genes KCNJ5, CACNA1D, CACNA1H, and CLCN2 can also occur in the germline, often at the identical positions affected by somatic mutations (8, 11, 12, 20–22). Such mutations cause an autosomal-dominant Mendelian disorder called familial hyperaldosteronism (FH). Additional cases are caused by mutations that create a chimeric CYP11B1/CYP11B2 gene (23). Patients with FH typically present with early-onset primary aldosteronism and hypertension. Collectively, these findings characterize primary aldosteronism as a largely genetic disorder, with somatic mutations in APAs and bilateral adrenal hyperplasia and germline mutations in FH.

This study focuses on CACNA1H, which we initially described as a disease gene for FH type IV (FH-IV) (11) in five unrelated kindreds. All carried the identical Met1549Val mutation. Whereas the five index cases all presented with hypertension by age 10 y and showed biochemical evidence of primary aldosteronism, two of five mutation-carrier relatives were normotensive, suggesting incomplete penetrance, as occasionally seen in FH (22). In one, both plasma renin activity and aldosterone levels were normal, in the other, plasma renin activity was at the lower limit of normal, and aldosterone was normal. Upon noncurative removal of one adrenal gland in a clinically affected mutation carrier, microscopic glomerulosa hyperplasia was observed. Daniil et al. (24) identified a different de novo mutation at the identical position (Met1549Ile) in a patient with early-onset primary aldosteronism and multiplex developmental disorder, along with other variants of less certain pathogenicity. More recently, Nanba et al. (10) found three adenomas with somatic Ile1430Thr CACNA1H mutations in a cohort of 75 APAs, establishing them as a rare cause of APAs.

CACNA1H encodes the T-type calcium channel α-subunit Ca$_V$3.2. T-type calcium channels activate at membrane potentials positive to −70 mV. A steady-state so-called window current occurs at potentials slightly positive to the glomerulosa resting membrane potential at which channels activate, but do not inactivate completely. It has been suggested that this property, together with oscillations in the zona glomerulosa membrane potential, allows Ca$_V$3.2 to transduce the calcium current that is necessary for aldosterone production (25). Like other calcium channel α-subunits, Ca$_V$3.2 contains four repeats, each with six transmembrane segments, and Met1549 mutated in FH-IV is located in the S6 segment of repeat III. Its mutation causes loss of normal channel inactivation and a slight shift of activation to less-depolarizing potentials (11), which in an adrenocortical cancer cell model is associated with increased aldosterone production (26).

Thus, strong evidence links CACNA1H mutations to primary aldosteronism. Yet, potential effects of CACNA1H gain-of-function mutations on adrenal cell mass (11) or on calcium signaling in the zona glomerulosa have not been studied.

Herein, we generated and characterized a mouse model carrying a heterozygous knockin mutation at a position that is homologous to human Met1549 (Cacna1h$^{M1560V/+}$). These mice showed an elevated ARR and elevated systolic and mean arterial blood pressure as signs of mild primary aldosteronism, but glomerulosa histology was normal. Intracellular glomerulosa calcium concentrations were elevated. We also used a corresponding knockout model (Cacna1h$^{-/-}$) to further investigate the physiological role of Ca$_V$3.2 in the adrenal gland.

Results

Generation and Characterization of Cacna1h$^{M1560V/+}$ and Cacna1h$^{-/-}$ Mice.
The protein sequences of the Ca$_V$3.2 S6 helix in repeat III, including the location of the p.Met1549Val mutation in humans, are completely conserved between human and mouse (11). In addition, the genomic sequences are identical at the triplet encoding Met1549 in humans and the corresponding Met1560 (NM_021415.4) in mice (Fig. 1A). We used CRISPR/Cas9-based genome editing to introduce the p.Met1560Val mutation on exon 25 of the Cacna1h gene into the mouse genome (Fig. 1B). Evaluation of different single-guide RNAs (sgRNAs) by simultaneous injection with Cas9 mRNA into fertilized eggs, culturing to blastocyst, and genotyping (SI Appendix, Supplementary Methods) led to the identification of an sgRNA that caused insertions and deletions in 67% of cultured embryos. We coinjected this sgRNA with Cas9 mRNA and a donor oligonucleotide (repair template) and obtained mice carrying the p.Met1560Val mutation (Cacna1h$^{M1560V/+}$). One of these mice carried an 8-bp deletion causing a frameshift and termination codon (p.His1570Glnfs*83, Cacna1h$^{+/-}$) in trans. We performed backcrossing and further bred Cacna1h$^{+/-}$ mice to obtain homozygous knockout mice (Cacna1h$^{-/-}$). Both mutant alleles were expressed in adrenal cDNA (Fig. 1C).

Male and female Cacna1h$^{M1560V/+}$ and Cacna1h$^{+/-}$ mice were viable and fertile (SI Appendix, Fig. S1 A–C), and we did not observe obvious phenotypic abnormalities. However, when Cacna1h$^{+/-}$ were intercrossed, the number of Cacna1h$^{-/-}$ offspring was lower than the number of wild-type (WT) offspring, pointing to potential reduced fitness of the homozygous knockout (WT, n = 48, expected: 45; Cacna1h$^{+/-}$: n = 107, expected: 90 and Cacna1h$^{-/-}$: n = 25, expected: 45; P = 0.0021; χ^2 test, DF = 2) (SI Appendix, Fig. S1D), in line with a recent report (27). Constitutively constricted coronary arterioles and focal myocardial fibrosis have been described in a previously established Cacna1h knockout model (28, 29). We stained hearts of 48- to 60-wk-old WT, Cacna1h$^{M1560V/+}$ and Cacna1h$^{-/-}$ mice with Sirius red to identify fibrotic areas. While some fibrotic areas were identified, they were not exclusive to knockout animals (SI Appendix, Fig. S2).

Reduced Survival in Cacna1h$^{M1560V/M1560V}$ Mice.
We also intercrossed Cacna1h$^{M1560V/+}$ mice. Among 27 resulting litters, 117 mice survived until weaning and were genotyped. This revealed 40 WT mice, 76 Cacna1h$^{M1560V/+}$ mice, and 1 Cacna1h$^{M1560V/M1560V}$ mouse (SI Appendix, Fig. S1D); the single Cacna1h$^{M1560V/M1560V}$ mouse died shortly after weaning. The likelihood of seeing one or fewer Cacna1h$^{M1560V/M1560V}$ mice among 117 offspring by chance is 9.64×10^{-14} (binomial distribution probability). Next, we genotyped 25 pups from two additional litters incidentally found dead shortly after delivery and two litters killed shortly after birth. Of these neonates, five were WT, nine Cacna1h$^{M1560V/+}$, and nine Cacna1h$^{M1560V/M1560V}$. The discovery of many Cacna1h$^{M1560V/M1560V}$ mice among neonates together with the unexpectedly low number of homozygous mice at weaning suggests that Cacna1h$^{M1560V/M1560V}$ mice succumb to perinatal or early postnatal lethality. We did not observe obvious external malformations or lower weight in homozygous knockin pups. Because FH-IV is an autosomal-dominant disorder, we proceeded to characterize heterozygous knockin mice (Cacna1h$^{M1560V/+}$).
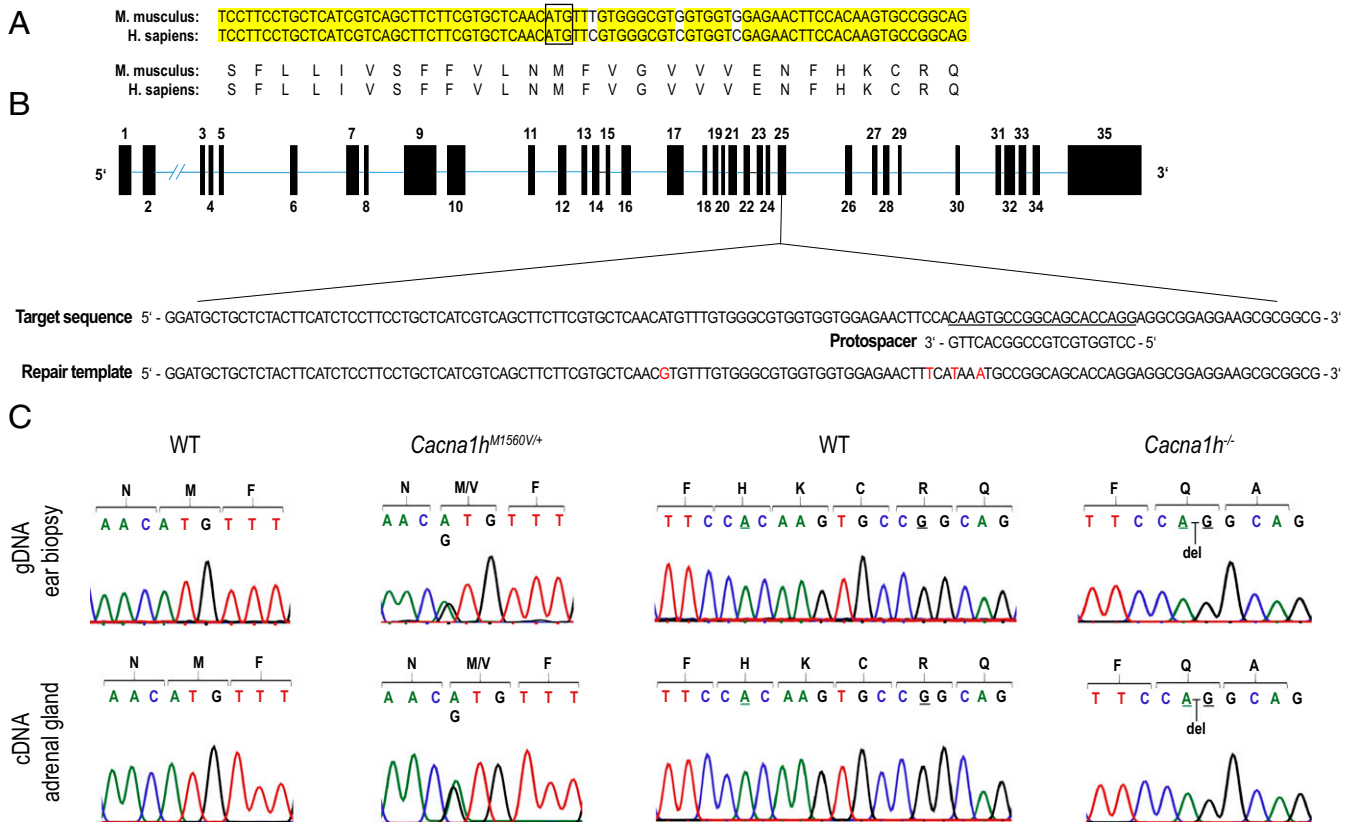
Fig. 1. Generation of *Cacna1h*[M1560V/+] and *Cacna1h*^{−/−} mouse models. (*A*) Alignment of *Mus musculus* and *Homo sapiens* genomic and amino acid sequences surrounding human Met1549 (box) mutated in FH-IV. Identical nucleotides are shown in yellow. The protein sequence is completely conserved. (*B*) Representation of the mouse *Cacna1h* locus targeted on exon 25. Sequences of protospacer used to target Cas9 nuclease to exon 25 and repair template used to introduce *Cacna1h*[M1560V/+] via homology-directed repair are listed below target sequence. The guide binding site is underlined, and intended mutations (including three silent mutations) are shown in red letters. (*C, Upper*) Sanger sequences of genomic DNA (gDNA, from ear biopsies) from a WT control, a *Cacna1h*[M1560V/+] mouse, and a *Cacna1h*^{−/−} mouse (knockout). (*Lower*) Sanger sequences of adrenal complementary DNA (cDNA) from the identical animals shown above, demonstrating adrenal expression of the mutant alleles. Bases adjacent to the 8-bp deletion in *Cacna1h*^{−/−} are underlined.

Normal Zona Glomerulosa Morphology in *Cacna1h*[M1560V/+] and *Cacna1h*^{−/−} Mice. To assess whether *Cacna1h* mutations cause macroscopic or microscopic glomerulosa hyperplasia, we harvested adrenal glands from *Cacna1h*[M1560V/+] mice, *Cacna1h*^{−/−} mice, and WT littermates of *Cacna1h*[M1560V/+] mice. There was no significant difference in adrenal weight (Fig. 2*A*). The presence of the Met1560Val mutation also had no effect on *Cacna1h* expression levels by real-time PCR (Fig. 2*B*), and subgroup analysis identified no difference in *Cacna1h* expression in either male or female mice (Fig. 2*C*). By in situ hybridization, we identified *Cacna1h* staining in the zona glomerulosa, and also the zona fasciculata (*SI Appendix*, Fig. S3). H&E staining demonstrated unaltered adrenal zonation in *Cacna1h*[M1560V/+] and *Cacna1h*^{−/−} mice compared to WT (Fig. 2 *D* and *E*). Next, we performed in situ hybridization for *Cyp11b2* (a marker of zona glomerulosa) in knockin and knockout mice, as well as controls (Fig. 3). The fraction of *Cyp11b2*^{+} adrenal cells in the adrenal gland was unchanged in *Cacna1h*[M1560V/+] and *Cacna1h*^{−/−} mice compared to WT, but the staining intensity per cell was increased in *Cacna1h*[M1560V/+] mice (*SI Appendix*, Fig. S4). *Cyp11b2* expression was only detected in the zona glomerulosa, and we did not observe formation of microscopic *Cyp11b2*[+] nodules. Similarly, adrenal morphology of *Cacna1h*[M1560V/+] at ages 48 to 60 wk was unaltered compared to WT (*SI Appendix*, Fig. S5). Aged *Cacna1h*[M1560V/+] mice frequently showed hydronephrosis (*SI Appendix*, Fig. S6) [an occasional finding in aged laboratory mice (30), present in five of six *Cacna1h*[M1560V/+] animals vs. zero of four (nonlittermate) WT animals

and one of five *Cacna1h*^{−/−} mice, $P = 0.011$ for *Cacna1h*[M1560V/+] vs. both other genotypes combined, two-tailed Fisher's exact test].

***Cacna1h*[M1560V/+] Mice Have Elevated *Cyp11b2* Expression at Baseline and upon High-Salt Diet as Well as Elevated ARRs.** We next assessed adrenal *Cyp11b2* expression by quantitative real-time PCR (Fig. 4 *A–C*). *Cacna1h*[M1560V/+] mice had higher relative *Cyp11b2* levels than WT littermates (1.60 ± 0.98 in *Cacna1h*[M1560V/+] vs. 1.09 ± 0.44 in controls, mean $\pm$ SD throughout *Results* unless otherwise indicated, $P = 0.004$) (Fig. 4*A*; see legend for statistical tests). Subgroup analysis demonstrated significantly elevated values in male mice only (1.78 ± 0.95 in *Cacna1h*[M1560V/+] vs. 1.08 ± 0.43 in controls, $P = 0.004$) (Fig. 4*B*). A trend of elevated plasma aldosterone levels in the overall group was explained by significantly elevated values in male mice (276.0 ± 108.6 pg/mL in *Cacna1h*[M1560V/+] vs. 200.5 ± 122.7 pg/mL in controls, $P = 0.016$) (Fig. 4 *D* and *E* and Table 1). To clarify whether aldosterone levels in mutant mice were susceptible to RAS suppression, we fed mice a 4-wk high-salt diet (HSD; 1.71% sodium chow, 1% NaCl in drinking water). *Cyp11b2* levels were incompletely suppressed in *Cacna1h*[M1560V/+] mice on HSD compared to controls, suggesting relative autonomy (4.53 ± 3.02 in *Cacna1h*[M1560V/+] vs. 1.23 ± 0.89 in WT littermates, $P = 0.008$) (Fig. 4*C*). There was no significant difference in aldosterone levels (44.4 ± 15.0 pg/mL in *Cacna1h*[M1560V/+] vs. 37.1 ± 19.2 pg/mL in controls, $P = 0.393$) (Fig. 4*F*).

C57BL/6 mice have only one renin gene (*Ren1*) (31). We measured renal *Ren1* expression levels by quantitative real-time PCR
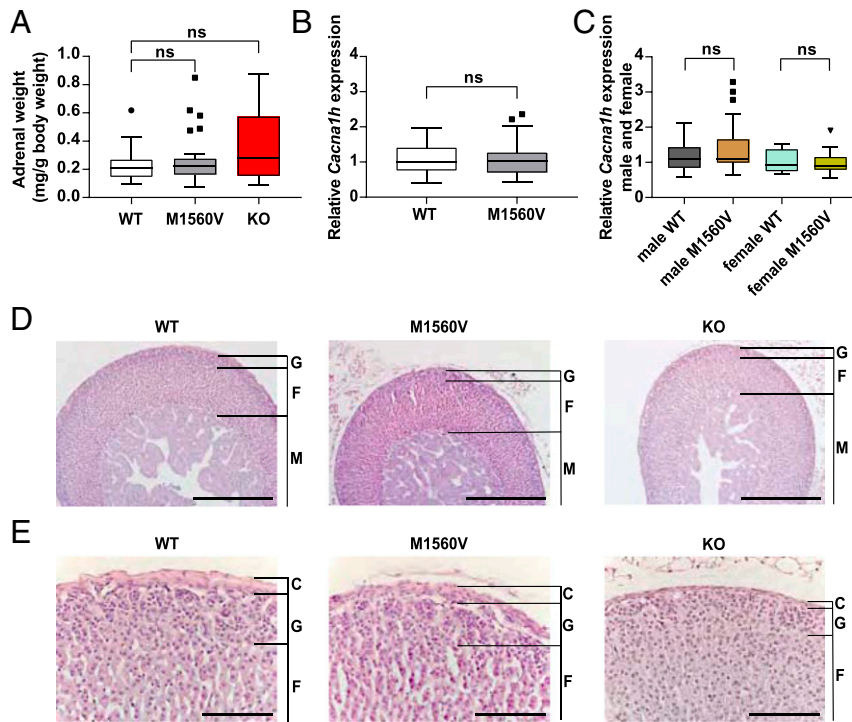
Seidel et al.
Enhanced Ca^{2+} signaling, mild primary aldosteronism, and hypertension in a familial hyperaldosteronism mouse model (*Cacna1h*[M1560V/+])

PNAS | 3 of 11
https://doi.org/10.1073/pnas.2014876118

Fig. 2. Adrenal glands of *Cacna1h*$^{M1560V/+}$ and *Cacna1h*$^{-/-}$ mice show unchanged morphology. (*A*) Adrenal weight (normalized to body weight) is unchanged between WT, *Cacna1h*$^{M1560V/+}$, and *Cacna1h*$^{-/-}$ mice (WT: *n* = 21; M1560V: *n* = 29; *P* = 0.69; knockout [KO]: *n* = 17; *P* = 0.17; Kruskal–Wallis test with Dunn's multiple comparisons test [MCP]). (*B*) Adrenal expression of *Cacna1h* is not changed in *Cacna1h*$^{M1560V/+}$ compared to WT (M1560V: *n* = 41; WT: *n* = 40; *P* = 0.95; unpaired two-tailed *t* test of log-transformed fold-change). (*C*) *Cacna1h* expression is unchanged between WT and *Cacna1h*$^{M1560V/+}$ in both sexes (male WT: *n* = 24; male M1560V: *n* = 17; *P* > 0.99; female WT: *n* = 16; female M1560V: *n* = 24; *P* > 0.99; Kruskal–Wallis test with Dunn's MCP of log-transformed fold-change). All data are shown as box plots (box, interquartile range; whiskers, 1.5 times the interquartile range; line, median; dots, outliers); *n* values represent animals. ns, *P* > 0.05. (*D* and *E*) H&E staining of adrenal sections show unaltered morphology of *Cacna1h*$^{M1560V/+}$ and *Cacna1h*$^{-/-}$ mice compared to WT (three mice each, representative images, pictures of male mice at 15 to 16 wk of age are shown). C, capsule; F, fasciculata; G, glomerulosa; M, medulla. (Scale bars, 500 μm in *D* and 100 μm in *E*.)

(Fig. 5 *A–C*). *Ren1* expression was not significantly changed in *Cacna1h*$^{M1560V/+}$ mice compared to WT littermates (Fig. 5*A*), and subgroup analysis similarly revealed no significant changes in male and female subgroups (Fig. 5*B*). Corresponding plasma renin concentrations (PRCs) were only significantly lower in female *Cacna1h*$^{M1560V/+}$ mice compared with WT mice (2,204 ± 1,008 ng/mL/h in *Cacna1h*$^{M1560V/+}$ vs. 3,290 ± 1,505 ng/mL/h in controls, *P* = 0.0463) (Fig. 5*E*), and similar tendencies were seen in males and in the overall analysis (Fig. 5*D*).

After HSD, *Ren1* expression was not significantly different between genotypes (Fig. 5*C*), but *Cacna1h*$^{M1560V/+}$ mice had lower PRCs than WT mice (973 ± 649 ng/mL/h in *Cacna1h*$^{M1560V/+}$ vs. 3,734 ± 2,503 ng/mL/h in controls, *P* = 0.0081) (Fig. 5*F*).

We calculated a *Cyp11b2:Ren1* expression ratio analogous to the ARR using the respective fold-changes. This ratio was significantly elevated in *Cacna1h*$^{M1560V/+}$ mice compared to controls both on a normal-salt diet (NSD; 2.73 ± 3.01 in *Cacna1h*$^{M1560V/+}$ vs. 1.22 ± 0.933 in controls, *P* = 0.005) (Fig. 5*G*) and on an HSD (6.48 ± 6.97 in *Cacna1h*$^{M1560V/+}$ vs. 1.33 ± 0.747 in controls, *P* = 0.009) (Fig. 5*I*). In NSD subgroup analysis, this effect was only significant in male mice (2.32 ± 1.48 in *Cacna1h*$^{M1560V/+}$ vs. 1.23 ± 0.983 in controls, *P* = 0.01) (Fig. 5*H*). The corresponding ARR was similarly elevated both on an NSD (0.250 ± 0.313 pg/mL:ng/mL/h in *Cacna1h*$^{M1560V/+}$ vs. 0.131 ± 0.139 pg/mL:ng/mL/h in controls, *P* = 0.0326) (Fig. 5*J*) and on an HSD (0.064 ± 0.039 pg/mL:ng/mL/h in *Cacna1h*$^{M1560V/+}$ versus 0.023 ± 0.021 pg/mL:ng/mL/h in controls, *P* = 0.0148) (Fig. 5*L*). Subgroup analysis of male and female mice on NSD did not show significant changes even though similar tendencies were seen (Fig. 5*K*).

Cacna1h$^{-/-}$ Mice Have Normal Adrenal Cyp11b2 and Plasma Aldosterone, but Elevated Renal Ren1 Levels. *Cyp11b2* levels and plasma aldosterone levels were unchanged in *Cacna1h*$^{-/-}$ mice compared with WT (Fig. 4 *A* and *D*). Whereas renal *Ren1* expression was significantly elevated (1.86 ± 0.86 in *Cacna1h*$^{-/-}$ versus 1.15 ± 0.59 in WT, *P* = 0.026) (Fig. 5*A*), PRC and ARR did not show significant changes compared to WT (Fig. 5 *D*, *G*, and *J*).

Cacna1h$^{M1560V/+}$ Mice Show Normal Plasma and Urinary Electrolytes. We did not measure significant differences in plasma potassium, sodium, or chloride levels in *Cacna1h*$^{M1560V/+}$ mice compared with WT (*SI Appendix*, Fig. S7 *A–C*). In spot urine, potassium/creatinine ratio, sodium/creatinine ratio, and chloride/creatinine ratios similarly did not show significant differences (*SI Appendix*, Fig. S7 *D–F*). Because aldosterone levels were normal in *Cacna1h*$^{-/-}$ mice, we did not assess serum or urinary electrolytes in these animals.

Elevated Blood Pressure in Cacna1h$^{M1560V/+}$ Mice. We performed invasive blood pressure monitoring in unanesthetized male mice by telemetry using carotid artery catheterization and analyzed data using a linear mixed model approach (*Materials and Methods* and Fig. 6). Systolic blood pressure (SBP; *P* = 0.0010) and mean arterial blood pressure (MAP; *P* = 0.0017) were elevated by a mean of 8.3 and 5.4 mmHg, respectively, in male knockin mice compared to WT littermates. Diastolic blood pressure (DBP; *P* = 0.1394) and heart rate were not significantly changed. Next, we fed animals an HSD and recorded blood pressure. Similar to the finding on an NSD, SBP and MAP were significantly elevated in knockin mice compared with WT controls, whereas DBP and heart rate showed no significant differences between genotypes.
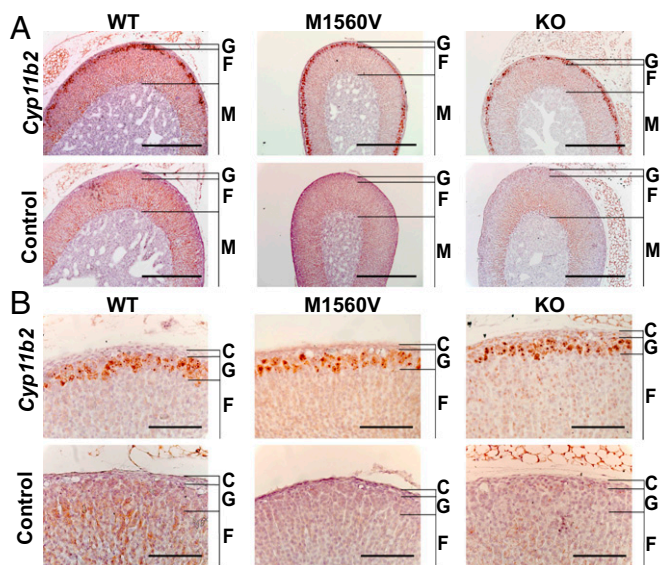
Seidel et al.
Enhanced Ca^{2+} signaling, mild primary aldosteronism, and hypertension in a familial
hyperaldosteronism mouse model (*Cacna1h*$^{M1560V/+}$)

Fig. 3. Adrenal sections of $Cacna1h^{M1560V/+}$ and $Cacna1h^{-/-}$ mice show normal $Cyp11b2$ staining. (A and B) In situ hybridization with corresponding negative controls (see *Materials and Methods*). One of four to five animals of each genotype is shown. C: capsule; F: fasciculata; G, glomerulosa; M: medulla. (Scale bars, 500 μm in A and 100 μm in B.)

Because aldosterone levels were normal in $Cacna1h^{-/-}$ mice, we did not measure blood pressure in these animals.

$Cacna1h^{M1560V/+}$ Mice Have Elevated Baseline and Peak Zona Glomerulosa Calcium Levels. To understand on a cellular level how the Met1560Val mutation affects calcium signaling in the zona glomerulosa, we stained adrenal slices of $Cacna1h^{M1560V/+}$ mice and WT littermate controls with the fluorescent and cell-permeable calcium indicator Fura-2 AM (ratiometric, allowing to determine absolute intracellular calcium concentrations) (*SI Appendix,* Fig. S8). Individual glomerulosa cells showed spikes of elevated calcium concentrations. These spikes clustered in bursts of activity, with the calcium concentration returning to baseline in between bursts (Fig. 7 *A* and *B* and Movies S1 and S2). We determined intracellular calcium concentrations at baseline (violet in Fig. 7 *A* and *B*) and peak (red circles in Fig. 7 *A* and *B*) levels. In the absence of Ang II, spiking was very infrequent, precluding statistical analysis of peak values, but baseline calcium levels were significantly elevated in $Cacna1h^{M1560V/+}$ mice at both 3 and 5 mM K^+ (Fig. 7*C*). After addition of Ang II (20 and 1,000 pmol, respectively), spiking increased, and baseline and peak intracellular calcium levels were significantly elevated in $Cacna1h^{M1560V/+}$ mice, again both at 3 and at 5 mM K^+ (Fig. 7*C*). Similarly, mean overall calcium concentrations (taking into account concentrations at baseline and during spiking) in $Cacna1h^{M1560V/+}$ mice were higher than in controls at all conditions tested (3 and 5 mM extracellular K^+, each at 0, 20, and 1,000 pM Ang II) (Fig. 7*D*). To understand whether the shape of individual spikes was changed, we used Calbryte 520 AM (nonratiometric, higher temporal resolution) (*SI Appendix,* Fig. S9*A*). The kinetics of the rise to peak and the fall to baseline calcium concentrations were not significantly different between $Cacna1h^{M1560V/+}$ mice and WT mice (*SI Appendix,* Fig. S9 *B* and *C*).

Finally, the frequency of spiking was slightly lower in $Cacna1h^{M1560V/+}$ mice at supraphysiologic Ang II levels (1,000 pM) only (Fig. 7*E*), likely due to a combination of lower frequencies of spiking during bursts (*SI Appendix,* Fig. S10*A*), decreased burst lengths (*SI Appendix,* Fig. S10*B*), and decreased numbers of bursts (*SI Appendix,* Fig. S10*C*). Values and results of statistical tests for calcium imaging are shown in *SI Appendix,* Table S1. Because $Cacna1h$ is

also expressed in the zona fasciculata (*SI Appendix,* Fig. S3), we also investigated 340/385-nm ratios (positively correlating with the intracellular calcium concentration) in this zone. Intracellular zona fasciculata calcium levels were higher in $Cacna1h^{M1560V/+}$ mice than in WT mice (*SI Appendix,* Fig. S11).

Discussion

$Cacna1h^{M1560V/+}$ mice develop mild primary aldosteronism, with approximately twofold elevated ARRs compared to WT (Fig. 5 and Table 1) and an increase in systolic blood pressure of 8 mmHg (Fig. 6), but without significant effects on serum or urinary electrolytes (although changes may be more easily detected in 24-h urine than in spot urine) (*SI Appendix,* Fig. S7). We observed a similar, smaller trend (though not significant) for DBP, which is interesting because primary aldosteronism in humans can be associated with isolated systolic hypertension (32). The moderate elevation of blood pressure may explain why only a trend of lower PRC levels was observed (Fig. 5 and Table 1). In addition, PRC levels can be artificially high due to stress-induced secretion and hypovolemia as a result of blood collection. Unexpectedly high PRC levels in WT animals on an HSD (Fig. 5*F*) may be due to such confounders. Of note, *Ren1* expression is less affected by such acute stimuli (33).

Blood pressure elevation in the range we observed in knockin animals (8.3 mmHg systolic) is clinically significant; lowering SBP by 10 mmHg has been associated with an ~40% lower risk of death from stroke and 30% lower risk from ischemic heart or other vascular disease in humans (34). Contrary to a model with increased expression of aldosterone synthase (35), $Cacna1h^{M1560V/+}$ mice did not show salt sensitivity of blood pressure. The underlying reasons remain to be clarified.

The phenotype in our model is milder than that of human index cases (11). Importantly, due to selection bias, human index cases likely represent phenotypic extremes. Mutation-carrier family members are better representatives of the phenotypic disease spectrum than index cases. The absence of hypertension and biochemical evidence of primary aldosteronism in two of five mutation-carrier family members (see introduction) suggests a rather mild phenotype in humans, similar to that of the mouse model described here. The severe phenotype in some patients raises the question whether factors other than the germline mutation could play a role in determining disease severity. Interestingly, the single patient who underwent adrenalectomy and for whom histology was available showed microscopic glomerulosa hyperplasia with nodular invasion of the capsule (11), unlike the mice characterized here. Such hyperplasia may be due to additional somatic mutations, as in recently described aldosterone-producing cell clusters (17), and could contribute to more severe primary aldosteronism and hypertension in some patients. Conversely, previously unexplained incomplete penetrance (11) may be related to the absence of hyperplasia in other subjects.

Overall adrenal $Cyp11b2$ expression (by quantitative real-time PCR) was elevated in our mouse model, yet the fraction of $Cyp11b2^+$ cells in $Cacna1h^{M1560V/+}$ mice (by in situ hybridization) was normal (*SI Appendix,* Fig. S4*A*), and no histologic changes were observed, suggesting that individual glomerulosa cells express higher amounts of $Cyp11b2$. Accordingly, staining intensity per cell (by in situ hybridization) was increased in $Cacna1h^{M1560V/+}$ mice (*SI Appendix,* Fig. S4*B*), although this observation is qualitative due to signal amplification during staining (36).

As in another model of primary aldosteronism with $Clcn2$ gain-of-function mutation (37), changes in aldosterone were more pronounced in male than in female animals, possibly due to sex dimorphism in adrenocortical tissue renewal or changes during the estrus cycle that cause higher variability in female mice (38, 39). Contrary to $Cyp11b2$ levels, in the overall group, aldosterone was not significantly elevated, although a trend was seen (Fig. 4*D*). A potential limitation of aldosterone measurements in mice (similar
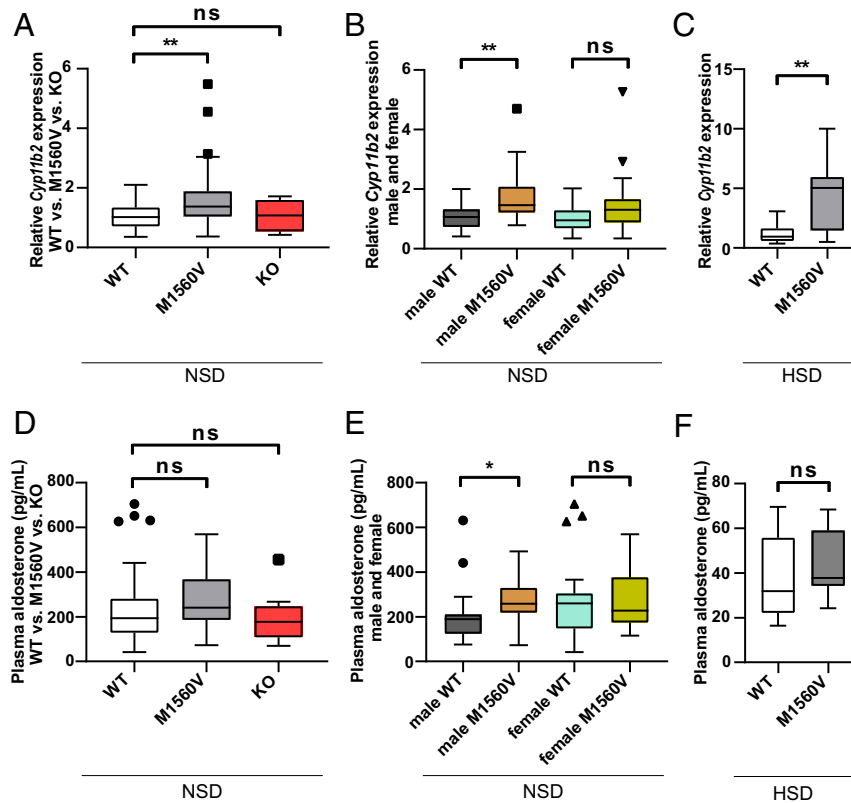
Seidel et al.
Enhanced Ca²⁺ signaling, mild primary aldosteronism, and hypertension in a familial hyperaldosteronism mouse model ($Cacna1h^{M1560V/+}$)

PNAS | 5 of 11
https://doi.org/10.1073/pnas.2014876118

Fig. 4. *Cacna1h*[M1560V/+] mice have elevated adrenal *Cyp11b2* expression. (*A*) Adrenal *Cyp11b2* expression is increased in *Cacna1h*[M1560V/+] mice during NSD (WT: $n = 43$; *Cacna1h*[M1560V/+]: $n = 43$; $P = 0.004$ vs. WT; KO: $n = 11$; $P = 0.996$ vs. WT; one-way ANOVA with Dunnett's MCP). (*B*) *Cyp11b2* expression is only increased in male *Cacna1h*[M1560V/+] mice (male WT: $n = 24$; male *Cacna1h*[M1560V/+]: $n = 18$; $P = 0.004$; female WT: $n = 19$; female *Cacna1h*[M1560V/+]: $n = 25$; $P = 0.294$; one-way ANOVA and Sidak's MCP). (*C*) Adrenal *Cyp11b2* expression remains elevated in *Cacna1h*[M1560V/+] mice during HSD (WT: $n = 12$; *Cacna1h*[M1560V/+]: $n = 9$; $P = 0.008$; unpaired two-tailed t test). (*D*) Plasma aldosterone is not significantly changed in *Cacna1h*[M1560V/+] mice or *Cacna1h*^{−/−} mice during NSD (WT: $n = 42$; *Cacna1h*[M1560V/+]: $n = 41$; $P = 0.090$; KO: $n = 13$; $P = 0.895$; Kruskal–Wallis test and Dunn's MCP). (*E*) Plasma aldosterone is significantly increased in male, but not in female *Cacna1h*[M1560V/+] mice (male WT: $n = 23$; male *Cacna1h*[M1560V/+]: $n = 17$; $P = 0.016$; female WT: $n = 19$; female *Cacna1h*[M1560V/+]: $n = 24$; $P > 0.999$; Kruskal–Wallis test and Dunn's MCP). (*F*) There is no significant difference in aldosterone between *Cacna1h*[M1560V/+] and WT during HSD (WT: $n = 8$; *Cacna1h*[M1560V/+]: $n = 9$; $P = 0.393$; unpaired two-tailed t test). Box plots (box, interquartile range; whiskers, 1.5 times the interquartile range; line, median; dots, outliers) are shown in the figure; n values are animals. ns, $P > 0.05$; *$P < 0.05$; **$P < 0.01$.

to renin measurements, see *Discussion* above) is the stress caused by the handling of animals prior to the blood draw, which can trigger aldosterone release (40).

Whether mice homozygous for the M1560V allele have more severe primary aldosteronism than heterozygous mice, as observed in a mouse model with N-terminal *Clcn2* deletion (41), could not be investigated due to apparent early lethality of homozygous mice. While the cause of lethality was not be established in this study, it would be interesting to assess whether homozygous *Cacna1h* knockin mice have evidence of severe hypertension at birth, which might, for example, manifest as cardiac hypertrophy. In heterozygous knockin mice, we did not detect target-organ damage (hypertensive nephropathy or cardiac abnormalities). Hydronephrosis may be a chance finding as it frequently occurs in aged mice (and WT controls of aged mice were not littermates). However, we note that Ca$_V$3.2 has been implicated in renal pacemaker activity, which triggers upper urinary tract peristalsis, moving urine from the kidney to the bladder (42).

T-type calcium channels are both activated and inactivated by voltage. The fraction of activated channels rises with increasing voltage in a sigmoidal fashion. In parallel, the fraction of channels that are not inactivated decreases in a sigmoidal fashion. The small voltage "window" in which these curves overlap allows for a small constitutive, noninactivating "window current" (see introduction). In channels with the Met1549Val mutation (in the human ortholog), we previously demonstrated by electrophysiology

that channel activation occurs at more negative membrane potentials (closer to the resting membrane potential of glomerulosa cells). As a result, the window current is larger than in WT channels (11). This larger constitutive current explains higher intracellular baseline glomerulosa calcium levels in *Cacna1h*[M1560V/+] mice (Fig. 7 *C* and *D*). In addition, impaired channel inactivation could lead to increased calcium influx at more depolarized potentials (i.e., during peaks). Interestingly, the spiking frequency was not elevated in *Cacna1h*[M1560V/+] mice, and even lower than in controls under some conditions (Fig. 7*E* and *SI Appendix*, Fig. S10*A*).

These findings are consistent with prior data suggesting that Ca$_V$3.2 is not the pacemaker in the depolarization phase of the oscillatory cycle. Ca$_V$3.2 current remains relatively constant and small in the interspike interval (25) (accounting for stably elevated baseline calcium levels in the mutant, see *Discussion* above). The initial depolarization that triggers rapid calcium influx during spikes must therefore be mediated by channels other than Ca$_V$3.2. Accordingly, a *Clcn2* gain-of-function mutation, which indirectly raises intracellular calcium via depolarization of glomerulosa cells, causes increased calcium spiking frequencies (37, 41). Lower frequencies under supraphysiological stimulation could be accounted for by two effects. First, recovery from inactivation is slower in channels carrying the Met1549Val mutation (11), and channels may take longer to be "available" for the next spike. Second, higher calcium levels in the presence of mutant channels could activate calcium-dependent potassium channels (43). Potassium current via

Seidel et al.
Enhanced Ca²⁺ signaling, mild primary aldosteronism, and hypertension in a familial
hyperaldosteronism mouse model (*Cacna1h*[M1560V/+])

Table 1. Characteristics of WT, $Cacna1h^{M1560V/+}$, and $Cacna1h^{-/-}$ mice

Parameter	WT	M1560V	KO	Male WT	Male M1560V	Female WT	Female M1560V
Plasma aldosterone (pg/mL)	237.9 ± 158.8 ($n = 42$)	274.1 ± 120.8 ($n = 41$)	196.2 ± 101.8 ($n = 13$)	200.5 ± 122.7 ($n = 23$)	276.0 ± 108.6* ($n = 17$)	283.2 ± 187.4 ($n = 19$)	272.7 ± 131.0 ($n = 24$)
PRC (ng/mL/h)	2733 ± 1700 ($n = 39$)	2038 ± 1150 ($n = 40$)	2325 ± 1138 ($n = 13$)	2303 ± 1748 ($n = 22$)	1813 ± 1316 ($n = 17$)	3290 ± 1505 ($n = 17$)	2204 ± 1008* ($n = 23$)
ARR (pg/mL:ng/mL/h)	0.13 ± 0.14 ($n = 39$)	0.25 ± 0.31* ($n = 39$)	0.08 ± 0.04 ($n = 13$)	0.15 ± 0.18 ($n = 22$)	0.37 ± 0.44 ($n = 17$)	0.1 ± 0.05 ($n = 17$)	0.16 ± 0.11 ($n = 22$)
Plasma K$^+$ (mmol/L)	4.66 ± 0.39 ($n = 11$)	4.57 ± 0.59 ($n = 14$)	N/A	4.94 ± 0.28 ($n = 5$)	4.78 ± 0.61 ($n = 9$)	4.42 ± 0.31 ($n = 6$)	4.17 ± 0.28 ($n = 5$)
Plasma Na$^+$ (mmol/L)	149.8 ± 2.11 ($n = 11$)	150.5 ± 2.35 ($n = 14$)	N/A	151.4 ± 2.06 ($n = 5$)	151.7 ± 1.78 ($n = 9$)	148.5 ± 0.83 ($n = 6$)	148.2 ± 1.16 ($n = 5$)
Plasma Cl$^-$ (mmol/L)	112.2 ± 1.44 ($n = 11$)	112.2 ± 1.44 ($n = 14$)	N/A	112.2 ± 1.41 ($n = 5$)	112.4 ± 1.55 ($n = 9$)	112.2 ± 1.60 ($n = 6$)	111.8 ± 1.28 ($n = 5$)
Urine K$^+$/Crea (mmol/L:mg/dL)	3.55 ± 2.72 ($n = 11$)	4.94 ± 3.12 ($n = 15$)	N/A	4.34 ± 2.88 ($n = 6$)	4.93 ± 2.57 ($n = 9$)	2.26 ± 1.60 ($n = 5$)	3.19 ± 1.28 ($n = 6$)
Urine Na$^+$/Crea (mmol/L:mg/dL)	2.05 ± 1.73 ($n = 11$)	3.91 ± 2.74 ($n = 15$)	N/A	2.56 ± 2.23 ($n = 6$)	3.73 ± 2.42 ($n = 9$)	1.36 ± 1.31 ($n = 5$)	3.16 ± 1.65 ($n = 6$)
Urine Cl$^-$/Crea (mmol/L:mg/dL)	2.85 ± 2.14 ($n = 11$)	4.61 ± 2.69 ($n = 15$)	N/A	3.65 ± 2.57 ($n = 6$)	4.53 ± 2.32 ($n = 7$)	1.77 ± 0.97 ($n = 5$)	3.65 ± 3.13 ($n = 6$)

M1560V, $Cacna1h^{M1560V/+}$; KO, $Cacna1h^{-/-}$; Crea, creatinine. All values on normal-salt diet. *$P < 0.05$ versus corresponding WT. All values given as mean ± SD. N/A, not available.

such channels would then hyperpolarize the cell and delay the next spike. Future pharmacologic studies could be instrumental to further investigate this effect. In any case, increased baseline and peak calcium levels result in a net increase in overall mean intracellular calcium levels (Fig. 7D), explaining the pathophysiology of FH-IV. Interestingly, intracellular calcium levels are elevated not only in the zona glomerulosa, but also the zona fasciculata of $Cacna1h^{M1560V/+}$ mice (*SI Appendix*, Fig. S11). While calcium may play a potentiating role, cAMP, downstream of ACTH, is the main stimulus of glucocorticoid production in the zona fasciculata (44). Given the rather mild effects of the Met1549Val mutation on aldosterone production, a major effect on glucocorticoid production appears unlikely, but was not investigated in this study. Hypercortisolism has not been reported in humans with FH-IV. Detailed studies were performed in one of the five index cases in the original description, demonstrating normal 24-h urinary free cortisol and normal ACTH (11).

Of further interest is the $Cacna1h^{-/-}$ mouse model. Ca$_V$3.2 has been proposed to be essential for intrinsic voltage oscillatory activity in the zona glomerulosa (25), raising the question whether inhibition of Ca$_V$3.2 could be a useful mechanism to lower blood pressure or aldosterone levels in the general population. Prior studies of another $Cacna1h^{-/-}$ model argue against such an effect, with normal aldosterone and renin levels and normal blood pressure (45). Similarly, Mibefradil, a calcium channel inhibitor that preferentially blocks T-type channels [withdrawn from the market (46)] does not have lasting effects on blood pressure or aldosterone levels (11, 47, 48) despite inhibitory effects in vitro (49). Our observations that *Cyp11b2* expression and aldosterone levels are not significantly changed in $Cacna1h^{-/-}$ mice (Fig. 4 *A* and *D*) support these prior findings and suggest that Ca$_V$3.2 is dispensable for aldosterone production in the zona glomerulosa in a chronic setting; elevated *Ren1* expression may suggest some degree of RAS activation. Thus, Ca$_V$3.2 inhibitors could possibly be used to treat patients with gain-of-function *CACNA1H* mutations (26), but are likely less suitable as a monotherapy for hypertension in the general population.

In summary, we have generated and characterized a mouse model of FH-IV, with mild primary aldosteronism. We show that primary aldosteronism in this model is due to higher baseline and peak intracellular calcium levels in the zona glomerulosa, caused by gain of Ca$_V$3.2 channel function. In a chronic setting, normal Ca$_V$3.2 appears to be dispensable for aldosterone production, perhaps because of compensatory mechanisms. It will be interesting to study in more detail the voltage and calcium oscillatory activity in the zona glomerulosa of $Cacna1h^{-/-}$ mice and characterize alternative calcium entry pathways.

Materials and Methods

Detailed methods are available in *SI Appendix*.

Generation of the $Cacna1h^{M1560V/+}$ Mouse Model. CRISPR/Cas-mediated mutation of *Cacna1h* Met1560 to Val was performed at the Yale Genome Editing Center, essentially as described previously (50).

Animals and Sample Collection. Mice were bred and housed at the Forschungseinrichtungen für Experimentelle Medizin (Charité - Universitätsmedizin Berlin). They were maintained under specific-pathogen free conditions in a 12-h light/dark cycle with ad libitum access to food and water. All animal experiments were approved by the local authorities (Landesamt für Gesundheit und Soziales Berlin) and performed under consideration of all relevant ethical regulations. Blood, tissue, and urine were collected as previously described (37).

Quantitative Real-Time PCR. Isolation of total RNA from adrenal glands and kidneys was done using the miRNeasy Mini Kit (Qiagen). Nanodrop 2000 (Thermo Scientific) was used for assessment of concentration and purity, and reverse transcription was done using Quantitect RT Kit (Qiagen). In adrenal cDNA, *Gapdh* (Mm99999915_g1, housekeeping gene) and *Cyp11b2* (Mm00515624_m1) were amplified using Taqman Gene Expression Master Mix (Applied Biosystems). *Gapdh* (primers 5′-TGTAGACCATGTAGTTGAGGTCA-3′ and 5′-AGGTCGGTGTGA-ACGGATTTG-3′), *Ren1* (5′-TCTGGGCACTCTTGTTGCTC-3′ and 5′-GGGGGAGGT-AAGATTGGTCAA-3′), and *Cacna1h* (5′-CGGCCCTACTACGCAGACTA-3′ and 5′-CCAGAGACTTGGGCTGGTTG-3′) were amplified from kidney and adrenal cDNA, respectively, using Power SYBR Green PCR Master Mix (Applied Biosystems). Gene expression was evaluated relative to *Gapdh* and mean ΔCT of WT controls and expressed as $2^{\Delta\Delta Ct}$ (fold-change).

H&E and Sirius Red Staining. H&E and Sirius red staining of formalin-fixed, paraffin-embedded (FFPE) adrenal glands, kidneys, and hearts was done as previously described (37).

In Situ Hybridization. *Cyp11b2* in situ hybridization was performed on 5-μm FFPE adrenal gland sections using the RNAscope 2.5 HD Assay-Brown (Advanced Cell Diagnostics) according to the manufacturer's instructions (document numbers: 322452 and 322310-USM). Probes were Mm-Cyp11b2 (Cat No. 505851), and DapB (Cat No. 310043, negative control).
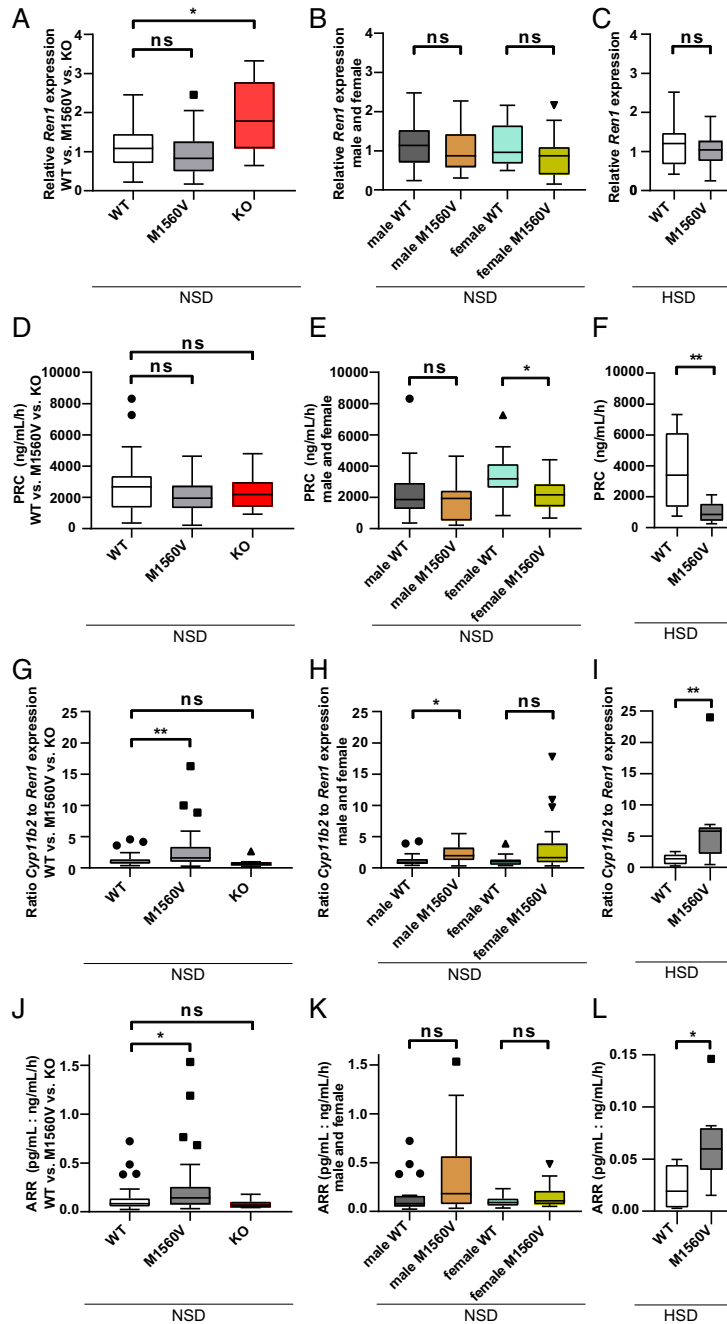
Seidel et al.
Enhanced Ca^{2+} signaling, mild primary aldosteronism, and hypertension in a familial hyperaldosteronism mouse model ($Cacna1h^{M1560V/+}$)

PNAS | 7 of 11
https://doi.org/10.1073/pnas.2014876118

Fig. 5. *Cacna1h*$^{-/-}$ mice show elevated *Ren1* expression; *Cacna1h*$^{M1560V/+}$ mice have elevated ARRs. (*A–C*) Kidney expression of *Ren1* is increased in KO mice but not significantly changed in *Cacna1h*$^{M1560V/+}$ mice during NSD (WT: n = 43; *Cacna1h*$^{M1560V/+}$: n = 43; P = 0.095 vs. WT; KO: n = 11; P = 0.026 vs. WT; one-way ANOVA and Dunnett's MCP; male WT: n = 24; male *Cacna1h*$^{M1560V/+}$: n = 18; P = 0.688; female WT: n = 19; female *Cacna1h*$^{M1560V/+}$: n = 25; P = 0.078; one-way ANOVA and Sidak's MCP) or HSD (WT: n = 12; *Cacna1h*$^{M1560V/+}$: n = 9; P = 0.425; Mann–Whitney test). (*D–F*) PRC is not significantly changed in *Cacna1h*$^{M1560V/+}$ and *Cacna1h*$^{-/-}$ mice during NSD (WT: n = 39; *Cacna1h*$^{M1560V/+}$: n = 40; P = 0.115; KO: n = 13; P > 0.999; Kruskal–Wallis test and Dunn's MCP). In subgroup analysis, PRC is decreased in female *Cacna1h*$^{M1560V/+}$ mice only (male WT: n = 22; male *Cacna1h*$^{M1560V/+}$: n = 17; P = 0.821; female WT: n = 17; female *Cacna1h*$^{M1560V/+}$: n = 23; P = 0.046; Kruskal–Wallis test and Dunn's MCP). PRC is reduced in *Cacna1h*$^{M1560V/+}$ mice during HSD (WT: n = 10; *Cacna1h*$^{M1560V/+}$: n = 8; P = 0.008; unpaired two-tailed t test). (*G–I*) The ratio of *Cyp11b2* and *Ren1* expression was calculated using fold-change. (*G*) Expression ratio is significantly increased in *Cacna1h*$^{M1560V/+}$ compared to WT mice and not significantly changed in *Cacna1h*$^{-/-}$ compared to WT (WT: n = 43; M1560V: n = 43; P = 0.005; *Cacna1h*$^{-/-}$: n = 11, P = 0.176; Kruskal–Wallis test, Dunn's MCP). (*H*) The ratio is significantly increased in male *Cacna1h*$^{M1560V/+}$ mice compared to WT (WT: n = 24; *Cacna1h*$^{M1560V/+}$: n = 18; P = 0.010; Kruskal–Wallis test and Dunn's MCP), but not in female mice (WT: n = 19; *Cacna1h*$^{M1560V/+}$: n = 25; P = 0.074; Kruskal–Wallis test and Dunn's MCP). (*I*) After HSD, the ratio is significantly increased in *Cacna1h*$^{M1560V/+}$ mice compared to WT (WT: n = 12; *Cacna1h*$^{M1560V/+}$: n = 9; P = 0.009; Mann–Whitney test). (*J*) ARRs (calculated using plasma aldosterone levels and PRC) are increased in *Cacna1h*$^{M1560V/+}$ mice compared to WT under NSD (WT: n = 39; M1560V: n = 39; P = 0.033; Kruskal–Wallis test with Dunn's MCP). In *Cacna1h*$^{-/-}$ mice, ARR is not significantly changed compared to WT (WT: n = 39; KO: n = 13; P = 0.540; Kruskal–Wallis test, Dunn's MCP). (*K*) ARR levels are not significantly changed in subgroup analyses (male WT: n = 22; M1560V: n = 17; P = 0.070; female mice WT: n = 17; M1560V: n = 22; P = 0.353; Kruskal–Wallis test, Dunn's MCP). (*L*) After HSD, ARR remains elevated in *Cacna1h*$^{M1560V/+}$ mice (WT: n = 8; *Cacna1h*$^{M1560V/+}$: n = 8; P = 0.015; unpaired two-tailed t test). All data are shown in box plots (box, interquartile range; whiskers, 1.5 times the interquartile range; line, median; dots, outliers); n values are animals. ns, P > 0.05; *P < 0.05; **P < 0.01.

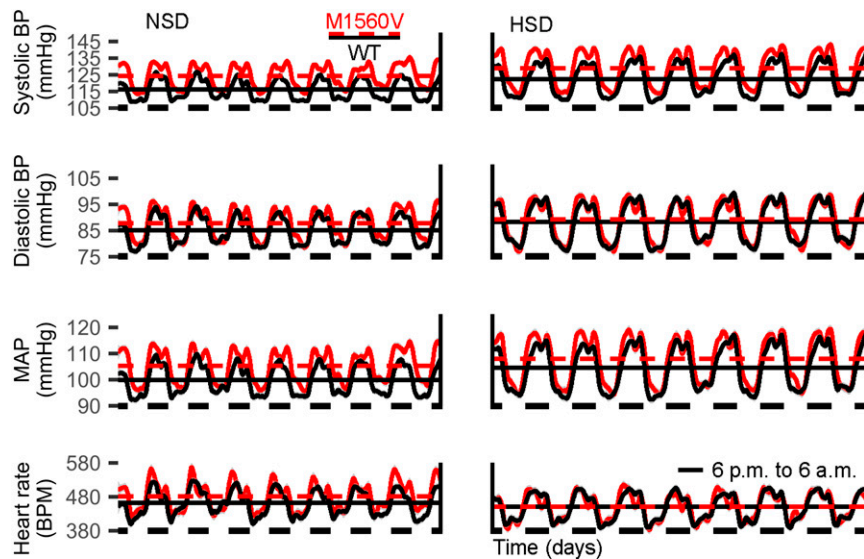**Fig. 6.** Blood pressure is higher in *Cacna1h*$^{M1560V/+}$ mice. Blood pressure (BP) and heart rate (HR) of animals were assessed during NSD and HSD through common carotid artery telemetry. Graphs show loess regressions of BP or HR of WT (black, $n = 8$ animals on NSD and $n = 7$ on HSD) and *Cacna1h*$^{M1560V/+}$ (red, $n = 7$ animals for both conditions) mice. Gray intervals denote 95% confidence intervals for loess regressions. Horizontal axis shows time, with black lines noting nights (6:00 PM to 6:00 AM). Horizontal lines show means for the entire NSD and HSD period, respectively, for WT (black) and *Cacna1h*$^{M1560V/+}$ (red dashed) animals. Nested-model likelihood ratio comparisons revealed significantly higher SBP ($P = 0.001$) and MAP ($P = 0.002$) during NSD; DBP ($P = 0.139$) and HR ($P = 0.135$) were not significantly changed. $n = 9$ WT, $n = 8$ *Cacna1h*$^{M1560V/+}$ animals. Mean ± SD values: NSD-SBP, 115.9 ± 13.7 mmHg (WT), 124.2 ± 14.7 mmHg (*Cacna1h*$^{M1560V/+}$); NSD-DBP, 85.0 ± 12.1 mmHg (WT) and 87.7 ± 11.9 mmHg (*Cacna1h*$^{1560V/+}$); NSD-MAP, 99.9 ± 12.5 mmHg (WT) and 105.2 ± 13.1 mmHg (*Cacna1h*$^{M1560V/+}$); NSD-HR, 462.2 ± 100.4 beats per minute (BPM, WT) and 482.1 ± 111.1 BPM (*Cacna1h*$^{M1560V/+}$). Similarly, during HSD, SBP ($P = 0.0008$) and MAP ($P = 0.021$) were increased in *Cacna1h*$^{M1560V/+}$ mice, while DBP ($P = 0.65$) and HR ($P = 0.92$) were unchanged. One WT mouse failed HSD recording. Mean ± SD: HSD-SBP, 122.2 ± 15.7 mmHg (WT) and 128.8 ± 18.1 mmHg (*Cacna1h*$^{M1560V/+}$); HSD-DBP, 88.2 ± 13.4 mmHg (WT) and 89.2 ± 13.7 mmHg (*Cacna1h*$^{M1560V/+}$); HSD-MAP, 104.5 ± 14.2 mmHg (WT) and 108.0 ± 15.4 mmHg (*Cacna1h*$^{M1560V/+}$); HSD-HR, 450.9 ± 92.3 BPM (WT) and 451.8 ± 100.9 BPM (*Cacna1h*$^{M1560V/+}$).

Microscopy. Pictures of adrenal glands (H&E staining and in situ hybridization) and hearts (Sirius red staining) were recorded with an Axioplan 2 microscope equipped with a Hal100 microscope lamp and an Axiocam MRc5 camera using Plan-Neofluar (5×, 10×, 40×) objectives and Axiovision Rel 4.8 software (all from Carl Zeiss). Pictures of whole kidneys (H&E staining) were recorded with an Axioscop 40 equipped with an Axiocam MRc5 and MCX-2eco high-resolution position controller using a Plan-Apochromat 20× objective and Axiovision Rel 4.8 software (all from Carl Zeiss).

Aldosterone ELISA. Plasma aldosterone concentration (pg/mL) was measured by enzyme-linked immunosorbent assay (ELISA, RE52301; IBL International) according to the manufacturer's instructions.

Determination of PRC. PRC was determined by measuring the capability of the sample to generate angiotensin I (AT-I) from excess renin substrate, as previously described (51).

Determination of Electrolytes. Plasma and urine electrolytes (K^+, Na^+, Cl^-) and urine creatinine were measured using an AU480 Clinical Chemistry Analyzer (Beckman Coulter) at the Animal Phenotyping Facility at Max-Delbrück-Centrum Berlin. Urine electrolyte concentrations were normalized to urine creatinine.

Blood Pressure Measurements. Blood pressure was measured via telemetry, as previously described (37).

Calcium Imaging. For slice preparation, adrenal glands were rapidly extracted from 12- to 18-wk-old mice (WT: 7 female and 9 male; M1560V: 10 female and 7 male mice) following anesthesia with isoflurane (1 mL as open drop) and cervical dislocation. The glands were then transferred into ice-cold bicarbonate-buffered saline (BBS: 119 mmol/L NaCl, 2 mmol/L KCl, 26 mmol/L NaHCO₃, 0.1 mmol/L CaCl₂, 5 mmol/L MgCl₂, 10 mmol/L glucose) gassed with carbogen (95% O₂ + 5% CO₂).

After removal of surrounding fat, both glands were embedded into 3% low-melting temperature agarose in BBS and glued to the mounting stage of a vibratome (7,000 smz-2; Campden Instruments). Organs in the agarose block were maintained in gassed BBS at temperatures below 4 °C at all times. Slices were cut at 70-μm thickness and transferred to BBS at 35 °C for 30 min for regeneration. Afterward, adrenal slices were stored for up to 6 h in BBS supplemented with 2 mmol/L CaCl₂ at room temperature (~22 °C).

Slice staining of adrenal slices was performed in a cell culture insert within a single well of a 24-well plate. The well was filled with 750 μL of BBS and the insert with 250 μL containing initially 64 μmol/L Fura-2 AM + 10% Pluronic F-127 dissolved in BBS. The well was continuously gassed with carbogen. Slices were left in the staining solution for 1 h followed by 15 min of de-esterification in BBS without Fura-2.

For recording, slices were placed in a recording chamber continuously perfused with solution from a reservoir supplied with carbogen gas. Two solutions were prepared and mixed to yield the potassium concentration of interest (BBS 2K⁺ : 119 mmol/L NaCl, 2 mmol/L KCl, 26 mmol/L NaHCO₃, 5 mmol/L NaGluconate, 2 mmol/L CaCl₂, 1 mmol/L MgCl₂, 10 mmol/L glucose; and BBS 7K⁺: 119 mmol/L NaCl, 2 mmol/L KCl, 26 mmol/L NaHCO₃, 5 mmol/L KGluconate, 2 mmol/L CaCl₂, 1 mmol/L MgCl₂, 10 mmol/L glucose). Ang II was added from a 1 mmol/L stock to the final concentration as indicated. Fura-2 fluorescence was alternately excited at 340 and 385 nm using a FuraLED light source (Cairn Research). Images were taken every 100 ms with 10-ms exposure using an OptiMOS camera (QImaging).

Statistics. Data were analyzed using GraphPad Prism 8 unless otherwise indicated.

Seidel et al.
Enhanced Ca²⁺ signaling, mild primary aldosteronism, and hypertension in a familial hyperaldosteronism mouse model (*Cacna1h*$^{M1560V/+}$)

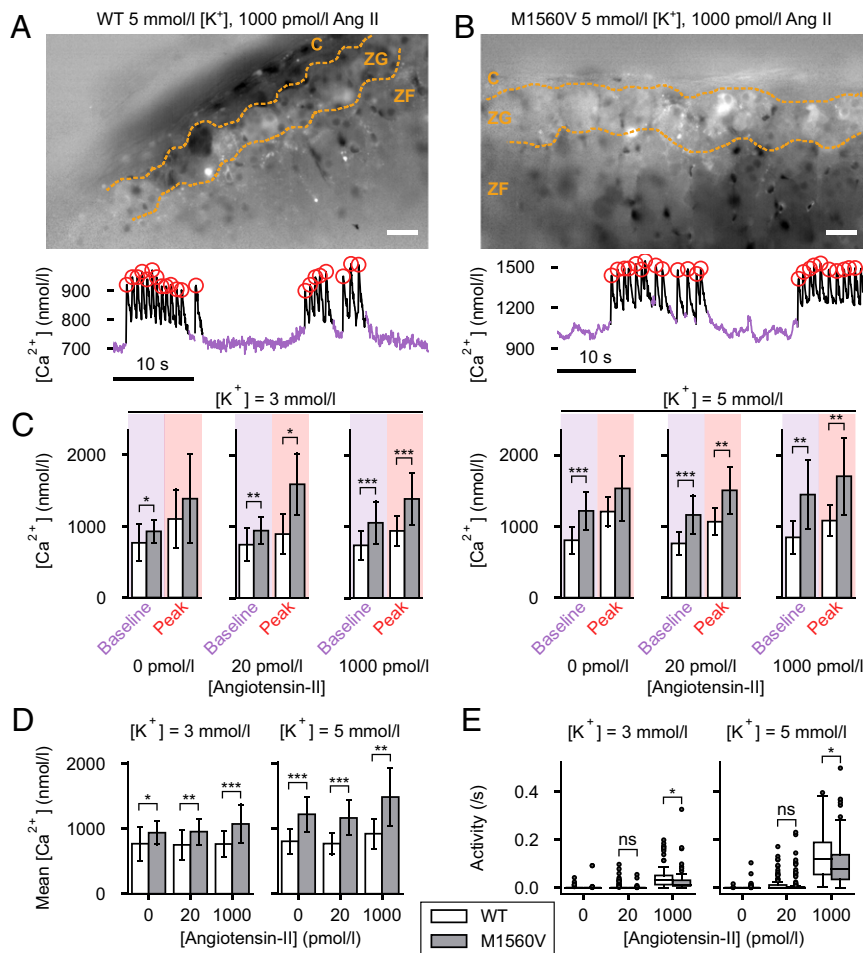PNAS | 9 of 11
https://doi.org/10.1073/pnas.2014876118

Fig. 7. *Cacna1h*$^{M1560V/+}$ mice have higher intracellular calcium concentrations than controls. (*A* and *B*) Representative average projections over 20 s from a WT or M1560V adrenal slice stained with Fura-2 AM (*Upper*). Intensity corresponds to the intracellular calcium concentration. (Scale bars, 10 μm.) The concentration changes of one representative cell each (both at 5 mM K$^+$ and 1 nM Ang II) are shown below. The trace is color-coded to represent baseline concentrations (purple), spiking activity (black) and peak concentrations (center of red circles). (*C*) Baseline as well as peak intracellular calcium concentrations are higher in *Cacna1h*$^{M1560V/+}$ compared to WT mice under all tested conditions. (*D*) The mean overall intracellular calcium concentrations (including baseline, spiking and peak segments) are also elevated in *Cacna1h*$^{M1560V/+}$ mice. (*E*) Mean frequencies of calcium spikes during the corresponding perfusions are lower in *Cacna1h*$^{M1560V/+}$ than in WT mice at supraphysiological concentrations of Ang II only. *P* values (likelihood ratio test of linear mixed models) are indicated as follows: ns, $P \geq 0.05$; *$P < 0.05$; **$P < 0.01$; ***$P < 0.001$. See SI Appendix, Table S1 for statistical information. Data in *C* and *D* are shown as bars (mean) ± SD. Data in *E* are shown in box plots (box, interquartile range; whiskers, 1.5 times the interquartile range; line, median; dots, outliers).

1. N. G. Hattangady, L. O. Olala, W. B. Bollag, W. E. Rainey, Acute and chronic regulation of aldosterone production. *Mol. Cell. Endocrinol.* **350**, 151–162 (2012).
2. A. Spät, L. Hunyady, Control of aldosterone secretion: A model for convergence in cellular signaling pathways. *Physiol. Rev.* **84**, 489–539 (2004).
3. S. Monticone et al., Prevalence and clinical manifestations of primary aldosteronism encountered in primary care practice. *J. Am. Coll. Cardiol.* **69**, 1811–1820 (2017).
4. J. W. Funder et al., The management of primary aldosteronism: Case detection, diagnosis, and treatment: An endocrine society clinical practice guideline. *J. Clin. Endocrinol. Metab.* **101**, 1889–1916 (2016).
5. K. Nanba et al., Targeted molecular characterization of aldosterone-producing adenomas in White Americans. *J. Clin. Endocrinol. Metab.* **103**, 3869–3876 (2018).
6. K. Nanba et al., Genetic characteristics of aldosterone-producing adenomas in Blacks. *Hypertension* **73**, 885–892 (2019).
7. K. De Sousa et al., Genetic, cellular, and molecular heterogeneity in adrenals with aldosterone-producing adenoma. *Hypertension* **75**, 1034–1044 (2020).
8. U. I. Scholl et al., Somatic and germline CACNA1D calcium channel mutations in aldosterone-producing adenomas and primary aldosteronism. *Nat. Genet.* **45**, 1050–1054 (2013).
9. E. A. Azizan et al., Somatic mutations in ATP1A1 and CACNA1D underlie a common subtype of adrenal hypertension. *Nat. Genet.* **45**, 1055–1060 (2013).
10. K. Nanba et al., Somatic *CACNA1H* mutation as a cause of aldosterone-producing adenoma. *Hypertension* **75**, 645–649 (2020).
11. U. I. Scholl et al., Recurrent gain of function mutation in calcium channel CACNA1H causes early-onset hypertension with primary aldosteronism. *eLife* **4**, e06315 (2015).
12. M. Choi et al., K+ channel mutations in adrenal aldosterone-producing adenomas and hereditary hypertension. *Science* **331**, 768–772 (2011).
13. R. K. Dutta et al., A somatic mutation in CLCN2 identified in a sporadic aldosterone-producing adenoma. *Eur. J. Endocrinol.* **181**, K37–K41 (2019).
14. F. Beuschlein et al., Somatic mutations in ATP1A1 and ATP2B3 lead to aldosterone-producing adenomas and secondary hypertension. *Nat. Genet.* **45**, 440–444, 444e1–2 (2013).
15. M. Tadjine, A. Lampron, L. Ouadi, I. Bourdeau, Frequent mutations of beta-catenin gene in sporadic secreting adrenocortical adenomas. *Clin. Endocrinol. (Oxf.)* **68**, 264–270 (2008).
16. E. Pignatti et al., Beta-Catenin causes adrenal hyperplasia by blocking zonal transdifferentiation. *Cell Rep.* **31**, 107524 (2020).
17. K. Nishimoto et al., Aldosterone-stimulating somatic gene mutations are common in normal adrenal glands. *Proc. Natl. Acad. Sci. U.S.A.* **112**, E4591–E4599 (2015).
18. K. Omata et al., Cellular and genetic causes of idiopathic hyperaldosteronism. *Hypertension* **72**, 874–880 (2018).

10 of 11 | PNAS
https://doi.org/10.1073/pnas.2014876118

Seidel et al.
Enhanced Ca^{2+} signaling, mild primary aldosteronism, and hypertension in a familial hyperaldosteronism mouse model (*Cacna1h*$^{M1560V/+}$)

19. C. E. Gomez-Sanchez, E. P. Gomez-Sanchez, K. Nishimoto, Immunohistochemistry of the human adrenal CYP11B2 in normal individuals and in patients with primary aldosteronism. *Horm. Metab. Res.* **52**, 421–426 (2020).
20. F. L. Fernandes-Rosa *et al.*, A gain-of-function mutation in the CLCN2 chloride channel gene causes primary aldosteronism. *Nat. Genet.* **50**, 355–361 (2018).
21. U. I. Scholl *et al.*, Hypertension with or without adrenal hyperplasia due to different inherited mutations in the potassium channel KCNJ5. *Proc. Natl. Acad. Sci. U.S.A.* **109**, 2533–2538 (2012).
22. U. I. Scholl *et al.*, CLCN2 chloride channel mutations in familial hyperaldosteronism type II. *Nat. Genet.* **50**, 349–354 (2018).
23. R. P. Lifton *et al.*, A chimaeric 11 beta-hydroxylase/aldosterone synthase gene causes glucocorticoid-remediable aldosteronism and human hypertension. *Nature* **355**, 262–265 (1992).
24. G. Daniil *et al.*, CACNA1H mutations are associated with different forms of primary aldosteronism. *EBioMedicine* **13**, 225–236 (2016).
25. C. Hu, C. G. Rusin, Z. Tan, N. A. Guagliardo, P. Q. Barrett, Zona glomerulosa cells of the mouse adrenal cortex are intrinsic electrical oscillators. *J. Clin. Invest.* **122**, 2046–2053 (2012).
26. E. N. Reimer, G. Walenda, E. Seidel, U. I. Scholl, CACNA1H mutant calcium channel causes autonomous aldosterone production in HAC15 cells and is inhibited by Mibefradil. *Endocrinology* **157**, 3016–3022 (2016).
27. S. Alpdogan, R. Clemens, J. Hescheler, F. Neumaier, T. Schneider, Non-Mendelian inheritance during inbreeding of Ca$_v$3.2 and Ca$_v$2.3 deficient mice. *Sci. Rep.* **10**, 15993 (2020).
28. C. S. Chiang *et al.*, The Ca(v)3.2 T-type Ca(2+) channel is required for pressure overload-induced cardiac hypertrophy in mice. *Circ. Res.* **104**, 522–530 (2009).
29. C. C. Chen *et al.*, Abnormal coronary function in mice deficient in alpha1H T-type Ca2+ channels. *Science* **302**, 1416–1418 (2003).
30. D. A. Springer *et al.*, Investigation and identification of etiologies involved in the development of acquired hydronephrosis in aged laboratory mice with the use of high-frequency ultrasound imaging. *Pathobiol. Aging Age Relat. Dis.* **4**, 10.3402/pba.v4.24932 (2014).
31. P. B. Hansen *et al.*, Plasma renin in mice with one or two renin genes. *Acta Physiol. Scand.* **181**, 431–437 (2004).
32. Z. Xu *et al.*; Chongqing Primary Aldosteronism Study (CONPASS) Group, Primary aldosteronism in patients in China with recently detected hypertension. *J. Am. Coll. Cardiol.* **75**, 1913–1922 (2020).
33. M. Chen, J. Schnermann, R. L. Malvin, P. D. Killen, J. P. Briggs, Time course of stimulation of renal renin messenger RNA by furosemide. *Hypertension* **21**, 36–41 (1993).
34. S. Lewington, R. Clarke, N. Qizilbash, R. Peto, R. Collins; Prospective Studies Collaboration, Age-specific relevance of usual blood pressure to vascular mortality: A meta-analysis of individual data for one million adults in 61 prospective studies. *Lancet* **360**, 1903–1913 (2002).
35. N. Makhanova, J. Hagaman, H. S. Kim, O. Smithies, Salt-sensitive blood pressure in mice with increased expression of aldosterone synthase. *Hypertension* **51**, 134–140 (2008).
36. V. Trivedi, H. M. T. Choi, S. E. Fraser, N. A. Pierce, Multidimensional quantitative analysis of mRNA expression within intact vertebrate embryos. *Development* **145**, dev156869 (2018).
37. J. Schewe *et al.*, Elevated aldosterone and blood pressure in a mouse model of familial hyperaldosteronism with ClC-2 mutation. *Nat. Commun.* **10**, 5155 (2019).
38. W. F. Ganong, Reproduction and the renin-angiotensin system. *Neurosci. Biobehav. Rev.* **19**, 241–250 (1995).
39. A. Grabek *et al.*, The adult adrenal cortex undergoes rapid tissue renewal in a sex-specific manner. *Cell Stem Cell* **25**, 290–296.e2 (2019).
40. J. Manolopoulou *et al.*, A highly sensitive immunofluorometric assay for the measurement of aldosterone in small sample volumes: Validation in mouse serum. *J. Endocrinol.* **196**, 215–224 (2008).
41. C. Göppner *et al.*, Pathogenesis of hypertension in a mouse model for human CLCN2 related hyperaldosteronism. *Nat. Commun.* **10**, 4678 (2019).
42. R. Hurtado, C. S. Smith, Hyperpolarization-activated cation and T-type calcium ion channel expression in porcine and human renal pacemaker tissues. *J. Anat.* **228**, 812–825 (2016).
43. T. Yang *et al.*, Small-conductance Ca2+-activated potassium channels negatively regulate aldosterone secretion in human adrenocortical cells. *Hypertension* **68**, 785–795 (2016).
44. A. Spät, L. Hunyady, G. Szanda, Signaling interactions in the adrenal cortex. *Front. Endocrinol. (Lausanne)* **7**, 17 (2016).
45. A. D. Thuesen *et al.*, Deficiency of T-type Ca^{2+} channels Ca$_v$3.1 and Ca$_v$3.2 has no effect on angiotensin II-induced hypertension but differential effect on plasma aldosterone in mice. *Am. J. Physiol. Renal Physiol.* **317**, F254–F263 (2019).
46. M. E. Mullins *et al.*, Life-threatening interaction of mibefradil and beta-blockers with dihydropyridine calcium channel blockers. *JAMA* **280**, 157–158 (1998).
47. R. Schmitt *et al.*, Hemodynamic and humoral effects of the novel calcium antagonist Ro 40-5967 in patients with hypertension. *Clin. Pharmacol. Ther.* **52**, 314–323 (1992).
48. I. Ragueneau *et al.*, Comparison of sympathetic modulation induced by single oral doses of mibefradil, amlodipine, and nifedipine in healthy volunteers. *Clin. Pharmacol. Ther.* **69**, 122–129 (2001).
49. M. F. Rossier, E. A. Ertel, M. B. Vallotton, A. M. Capponi, Inhibitory action of mibefradil on calcium signaling and aldosterone synthesis in bovine adrenal glomerulosa cells. *J. Pharmacol. Exp. Ther.* **287**, 824–831 (1998).
50. N. L. Price *et al.*, Specific disruption of Abca1 targeting largely mimics the effects of miR-33 knockout on macrophage cholesterol efflux and atherosclerotic plaque development. *Circ. Res.* **124**, 874–880 (2019).
51. H. Wanka *et al.*, Cytosolic renin is targeted to mitochondria and induces apoptosis in H9c2 rat cardiomyoblasts. *J. Cell. Mol. Med.* **13**, 2926–2937 (2009).
52. E. Seidel *et al.*, Enhanced Ca^{2+} signaling, mild primary aldosteronism, and hypertension in a familial hyperaldosteronism mouse model (*Cacna1h$^{M1560V/+}$*). *Zenodo*. https://zenodo.org/record/4671006#.YG7Z8kgzZ24. Deposited 8 April 2021.
53. E. Seidel *et al.*, Enhanced Ca^{2+} signaling, mild primary aldosteronism, and hypertension in a familial hyperaldosteronism mouse model (*Cacna1h$^{M1560V/+}$*). *Zenodo*. https://zenodo.org/record/4672114#.YG8MGUgzZ24. Deposited 8 April 2021.

PHYSIOLOGY

Seidel et al.
Enhanced Ca^{2+} signaling, mild primary aldosteronism, and hypertension in a familial hyperaldosteronism mouse model (*Cacna1h$^{M1560V/+}$*)

PNAS | 11 of 11
https://doi.org/10.1073/pnas.2014876118